

Cluster analysis of muscle functional MRI data

Bruce M. Damon,¹ Danielle M. Wigmore,² Zhaohua Ding,¹ John C. Gore,¹ and Jane A. Kent-Braun²¹Department of Radiology and Radiological Sciences, Vanderbilt University, Nashville, Tennessee 37232; and²Department of Exercise Science, University of Massachusetts at Amherst, Amherst, Massachusetts, 01003

Submitted 20 February 2003; accepted in final form 20 May 2003

Damon, Bruce M., Danielle M. Wigmore, Zhaohua Ding, John C. Gore, and Jane A. Kent-Braun. Cluster analysis of muscle functional MRI data. *J Appl Physiol* 95: 1287–1296, 2003. First published May 23, 2003; 10.1152/jappphysiol.00178.2003.—Muscle functional magnetic resonance imaging (mfMRI) is frequently used to determine spatial patterns of muscle involvement in exercising humans. A frequent finding in mfMRI is that, even within synergistic muscle groups, signal intensity (SI) data from individual voxels can be quite heterogeneous. The purpose of this study was to develop a novel method for organizing heterogeneous mfMRI data into clusters whose members behave similarly to each other but distinctly from members of other clusters and apply it in studies of functional compartmentalization in the anterior compartment of the leg. An algorithm was developed that compared the SI time courses of adjacent voxels and grouped together voxels that were sufficiently similar. The algorithm's performance was verified by using simulated data sets with known regional differences in SI time courses that were then applied to experimental mfMRI data acquired from six male subjects (age 22.6 ± 0.9 yr, mean \pm SE) who sustained isometric contractions of the dorsiflexors at 40% of maximum voluntary contraction. The experimental data were also characterized by using a traditional analysis (user-specified regions of interest from a single image), in which the relative change in SI and the contrast-to-noise ratio [CNR; $100\% \times (SI_{\text{RESTING}} - SI_{\text{ACTIVE}}) / (\text{noise standard deviation})$] were measured. In general, clusters were found in areas in which the CNR exceeded 5. Cluster analysis made functional distinctions between regions of muscle that were not seen with traditional analysis. In conclusion, cluster analysis's use of the full SI time course provides more sensitivity to muscle functional compartmentation than traditional analysis.

transverse relaxation time constant; image processing; time series; exercise; dorsiflexors

DURING THE PAST 15 YEARS, muscle functional magnetic resonance imaging (mfMRI) has emerged as a promising tool for studying muscle involvement during exercise because it is sensitive to the spatial pattern and extent of muscle utilization. For example, mfMRI has been used to identify different muscle utilization patterns in novice and elite rowers (9) and in uphill and horizontal running (25). It has also been used to detect changes in muscle function consequent to clinical con-

ditions such as peripheral vascular disease (31). The interpretation of these data, however, is limited by the absence of a full theoretical understanding of which physiological variables produce the mfMRI response and how their contributions may differ during and after exercise.

Multiexponential relaxation analysis has shown that the major contribution to signal intensity (SI) changes in mfMRI is made by the increase in the transverse relaxation time constant (T2) of intracellular water protons (4, 22, 23). Proposed explanations for intracellular T2 increases include the accumulation of end products of cellular energy metabolism, which cause water to move into the cell (4, 21), decreased intracellular pH (4, 8), and water shifts from an intracellular compartment possessing a short T2 (~ 20 ms) to a second intracellular compartment having a longer T2 (~ 40 ms) (22, 23). Any of these possible explanations, acting alone or in concert with the others, suggests that the intracellular T2 increase results from changes in the chemical behavior of water resulting from increased flux through energy metabolism pathways. In keeping with the long time required for flux through these pathways to reach a steady rate (~ 2 – 3 min), these changes make up a slowly evolving, large-magnitude component of the mfMRI response (14).

Changes in the extracellular space also affect the SI in mfMRI. Increases in interstitial volume [such as those caused by exercise (24) or leg negative pressure (18)] increase SI in T2-weighted images (6, 18), although the low interstitial volume fraction diminishes the importance of these changes (4, 18). Recently, Hu et al. (12) showed through the injection of an extracellular contrast agent that postexercise hyperemia affects SI in T2-weighted images as well. Finally, changes in blood oxygenation during exercise (11) will alter the T2 of blood (27). Changes in the relaxation of these tissue water fractions will not affect the intracellular T2 unless there is rapid exchange between them and the intracellular space (15) or unless the magnetic susceptibility gradients around capillaries affect diffusing intracellular spins. Otherwise, the quantitative importance of extracellular changes to SI in mfMRI will depend on the pulse sequence and timings and the intercompartmental exchange rates.

Address for reprint requests and other correspondence: B. M. Damon, Dept. of Radiology and Radiological Sciences, Vanderbilt Univ. Medical Center, 1161 21st Ave. South-MCN CCC-1121, Nashville, TN 37232-2675 (E-mail: bruce.damon@vanderbilt.edu).

The costs of publication of this article were defrayed in part by the payment of page charges. The article must therefore be hereby marked "advertisement" in accordance with 18 U.S.C. Section 1734 solely to indicate this fact.

Exercise-induced changes in energy metabolism, intracellular and interstitial volumes, and blood volume and oxygenation have different time courses; the result is a complex temporal pattern of SI changes in serially obtained echo-planar images (2, 14, 19). Jenner et al. (14) reported an approximately exponential rise in SI during isotonic dorsiflexion exercise. Others (2, 19) have shown a more complex pattern to the SI changes during and after exercise, with (sometimes) an abrupt initial rise, a dip (possibly below baseline), a secondary rise, and continued increases after exercise. In addition to differences in the shape of the response over time, the magnitude of the response may be heterogeneous.

These differences in shape and magnitude can exist between or within individual muscles (2). Traditionally, these differences have been analyzed by using regions of interest (ROIs) drawn around individual muscles according to an a priori model. One assumption of traditional analysis is that the SI time course within each ROI is homogeneous. However, if this assumption were invalid, then traditional analysis would mask heterogeneities that exist on a smaller scale. Furthermore, traditional mfMRI analysis implicitly assumes a common regional organization of neural activation, perfusion, and/or other systemic variables, an assumption that is physiologically unlikely. Therefore, the purpose of this study was to develop and apply a model-independent method for organizing heterogeneous mfMRI data into clusters whose members behave similarly to each other but distinctly from members of other clusters. Such a method would be useful in identifying regionally varying patterns in the mfMRI SI time course that would otherwise be missed and would allow the temporal and spatial correlation of SI changes with other physiological and biophysical parameters altered by exercise.

METHODS

The Clustering Algorithm

The following considerations apply to simulated or actual spin-echo, T2-weighted echo-planar images of exercising muscle obtained serially during sustained exercise. For any image voxel i within an activated region of muscle, we assume that there exists a SI time course similar to one of those shown in Fig. 1. For any adjacent voxel j , we assume that the time course will have a similar magnitude and shape to that of i if the two regions of muscle are similar with respect to their metabolic characteristics, blood supply and oxygenation, and neural activation; otherwise, the magnitude and/or shape will differ. These concepts are illustrated in Fig. 1: curves A and B (and A and C) have similar shapes and are well correlated but differ in magnitude, curves B and C have similar shapes and magnitudes, and curve D differs from curves A – C in shape and magnitude. Nonphysiological sources for differences in the curves, such as noise, motion artifacts, partial volume effects, and inhomogeneous distributions of the radio frequency field and the quality factor of the coil, may also exist.

To quantify the similarity between i and j , we calculate a similarity index (S_{ij}) that considers differences in shape and magnitude. First, a time series (such as the exercise or postexercise period) containing imaging data is specified.

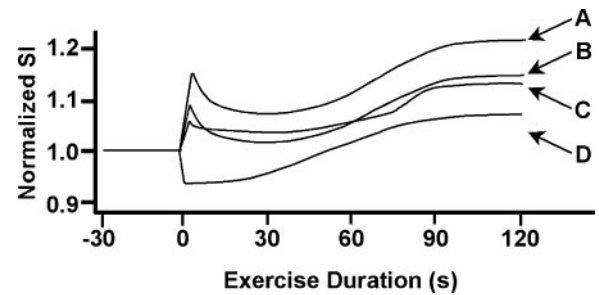


Fig. 1. Qualitative illustration of similar and dissimilar signal intensity (SI) time courses for individual voxels in muscle functional MRI (mfMRI) images during exercise. Curves B and C are similar to each other, but all other combinations differ in shape, magnitude, or both. SI time courses have been scaled to the preexercise mean.

Then, differences in the shapes of the two time series are quantified by calculating the Pearson's product-moment correlation (R_{ij}) between them; negative values of R_{ij} are set to zero. Because R_{ij} alone cannot distinguish between time series A and B in Fig. 1, the magnitude difference between the time series is also quantified, using the mean Euclidean distance (M_{ij}) between the two time series

$$M_{ij} = \frac{1}{N} \sum M_{ij,n} \quad (1)$$

where N is the number of images in the time series and $M_{ij,n}$ is the absolute difference in SI between i and j in the n th image, scaled to the range of muscle SI values encountered in that image. S_{ij} is calculated as

$$S_{ij} = (1 - M_{ij}^2) \cdot (R_{ij}^2) \quad (2)$$

Calculated in this way, similarity ranges from zero (least similar) to one (identical). Similar voxels are then grouped together by using the following procedure.

- 1) The eight voxels neighboring the voxel i are found. A planar ROI is defined within the image.
- 2) The similarity S between i and each of its neighbors is calculated.
- 3) Values of S lower than a threshold (T) are set to zero.
- 4) Up to K neighboring voxels are found whose non-zero similarities are greatest.
- 5) These voxels are grouped together into a cluster. This procedure is repeated for each voxel in the ROI. There are no limits to the size or number of individual clusters, except that provided by the definition of the ROI.

The resulting clusters can be classified as small (<5 voxels) or large (≥ 5 voxels). As stated above, the assignment of two voxels to separate clusters is assumed to reflect primarily a physiological difference between those two areas of muscle. It is also possible that noise could result in misassignment of a voxel. However, the algorithm employs several strategies for reducing the effects of noise. First, before S is calculated, the data from each voxel are filtered at 0.0625 Hz with a fifth-order low-pass Butterworth filter, which filters out high-frequency noise and preserves the low-frequency mfMRI data. Second, after the initial cluster assignment, small clusters are merged into adjacent clusters if the mean SI time courses from the clusters are sufficiently similar. The merging procedure is carried out as follows.

- 1) Cluster C is characterized as large or small.
 - 2A) If C is large, S is calculated between C and each adjacent small cluster. If $S > T$, the clusters together are merged together.
 - 2B) If C is small, S is calculated between C and all adjacent

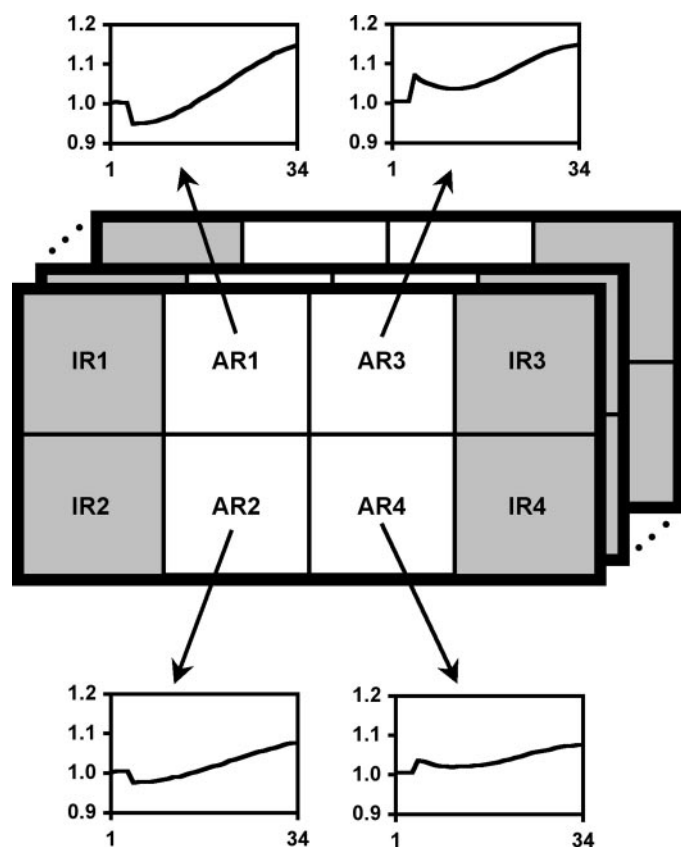


Fig. 2. Example cluster assignments in the simulations used for testing the algorithm. *Insets*: programmed exercise SI time courses for the active regions (AR1–4). In each *inset*, the abscissa is the matrix page number and the ordinate is scaled SI. AR1 and AR3 have relative changes in SI at end exercise of 15%, whereas AR2 and AR4 have relative changes in SI at end exercise of 7.5%; this corresponds to simulation condition C in Table 1. In the inactive regions (IR1–4), there are no changes in SI except those due to noise.

clusters. For any comparison in which $S > T$, the clusters are merged together. 3) These steps are repeated for all clusters in the data set, beginning with the smallest cluster and ending with the largest. This procedure is repeated for each voxel in the ROI. There are no limits to the size or number of individual clusters, except these provided by the definition of the ROI.

Simulation Studies

To test the algorithm and identify appropriate values of T and K , simulated data sets were tested by using MATLAB (The Mathworks, Natick, MA). Each data set contained 34 pages of 12×22 matrix; each page represented a different point in time (Fig. 2). In each page, the central 200 elements were organized into eight regions, with noise at the boundaries. There were four inactive (IR1–4) and four active (AR1–4) regions, each of size 5×5 . The inactive regions had unit SI in all 34 matrix pages. In AR1–4, the first four matrix pages simulated inactive muscle and the remaining 30 contained simulated mfMRI SI time series. AR1 and AR2 had SI time series similar to *curve D* in Fig. 1, whereas the time series in AR3 and AR4 were similar to *curves A–C* in Fig. 1. The simulated time series were generated by fitting typical experimentally obtained SI time series to third-order polynomials and solving for exercise durations of 4–120 s, in increments of 4 s. The third-order polynomial was chosen because

it fit the data well and does not imply a specific mechanism for SI changes in mfMRI. Gaussian noise was added to the time series to generate signal-to-noise ratios (SNRs) of 150, 200, or 250. These SNR levels are similar to those in experimental data (mean of 195, range of 155–237).

The spatial design of the matrix allowed testing between SI time series that differed in shape but had similar relative SI changes at the end of exercise. The algorithm’s ability to discriminate between SI time series with similar shapes but different magnitudes was also tested. To vary the magnitude, the fit SI values were scaled up or down to produce a specified end-exercise relative SI change (Table 1). In all, there were 15 different simulation conditions, each with a unique combination of SI and SNR.

To optimize T for experimental studies, repeated simulations were run. T was increased from 0.5 (in steps of 0.05) until $\geq 90\%$ classification accuracy (CA) was attained in each of six independent trials. The CA was calculated as

$$CA = 100\% \cdot \left(1 - \frac{(N_{N-} + N_{P-})}{N_R} \right) \quad (3)$$

where N_R is the programmed size of the region, N_{N-} is the number of false-negative voxel assignments, and N_{P-} is the number of false-positive voxel assignments. K was set to 4 in all of these trials. In addition, simulations were run to test the algorithm’s dependence on K . These simulations were run by using condition C200, with $T = 0.60$ and values of K ranging from 1 to 8.

Experimental Studies

Subjects. The studies were conducted at the Yale University MRI facility. The Institutional Review Boards of the University of Massachusetts at Amherst and the Yale University School of Medicine approved these studies. The subjects were seven apparently healthy, untrained male volunteers. Each subject provided written, informed consent before participating in the study. In one of the subjects, excessive leg movement during exercise precluded cluster analysis. The presentation and discussion of the data are restricted to the remaining six subjects (age = 22.6 ± 0.9 yr, height = 180.0 ± 2.0 cm, mass = 76.1 ± 3.1 kg).

Exercise protocol. The subjects sustained a 2-min isometric contraction of the right dorsiflexors at 40% of maximum voluntary contraction (MVC). The subjects lay supine on the patient bed of the imager with their right foot in an exercise apparatus. The leg was fully extended, and the foot was held in $\sim 30^\circ$ of plantar flexion. The exercise apparatus consisted of an aluminum plate, to which a load cell (model SSM-AJ-250, Interface, Scottsdale, AZ) was attached. The subjects

Table 1. Assignments of end-exercise relative SI changes in simulated data sets

Condition	AR1	AR2	AR3	AR4
A	15.0	2.5	15.0	2.5
B	15.0	5.0	15.0	5.0
C	15.0	7.5	15.0	7.5
D	15.0	10.0	15.0	10.0
E	15.0	12.5	15.0	12.5

The entries under active regions 1–4 (AR1–4) indicate the relative change in end-exercise signal intensities (SI) undergone by that region in 5 different conditions. Each condition was tested at signal-to-noise ratio (SNR) values of 150, 200, and 250. The combinations of condition and SNR are referred to as A150, A200, A250, and so forth. The spatial distribution of regions is described in Fig. 2.

pulled against a Velcro strap that was secured to the footplate. The plate and load cell were held within a wooden frame secured to the patient bed. The signals from the load cell were amplified (model SGA, Interface), digitized at 500 Hz by an analog-to-digital converter (DAQPAD-6020E, National Instruments, Austin, TX), and recorded on an IBM-compatible laptop computer using LabView version 5.1 (National Instruments). An output from LabView, proportional to relative contraction intensity, was displayed on an LED panel and enabled the subjects to maintain the desired contraction intensity.

Earlier in the test session, the subjects performed a series of procedures in which perfusion-sensitive images were obtained. The procedures included a single-cuff occlusion protocol in which a blood pressure cuff placed proximal to the knee was inflated to 220 mmHg for 5 min, two 10-s contractions to determine MVC, and ten 10-s submaximal contractions (two each at 10, 30, 50, 70, and 90% of MVC). These contractions were followed by another MVC to evaluate the possibility of fatigue. There were 5 min of rest between each of these procedures and before the 2-min contraction described above.

MR measurements. Imaging was performed on a 1.5-T whole-body Signa (GE Medical Systems, Milwaukee, WI) MR imager. Before exercise, contiguous multislice gradient-echo localizer scans were acquired in three planes and used to locate the maximum cross-sectional area of the anterior compartment. Subsequent imaging was performed with single-slice axial acquisitions at this location. A high-resolution, T₁-weighted conventional spin-echo image, used to define ROIs in the traditional mfMRI analysis (see below), was acquired by using repetition time (TR)/echo time (TE) = 600/14 ms, field of view = 20 cm, matrix = 256 × 256, slice thickness = 10 mm, and one excitation. mfMRI used T2-weighted, spin-echo axial echo-planar images acquired with TR/TE = 4,000/35 ms, field of view = 20 cm, matrix = 64 × 64, slice thickness = 10 mm, one excitation, and a 62.5-kHz bandwidth. Seventy mfMRI images were acquired: 4 before, 30 during, and 36 after exercise.

Image analysis. Image analysis was performed in MATLAB. To compensate partially for potential artifacts such as inhomogeneous distributions of the radio frequency field and quality factor of the coil, each voxel's SI time course was divided by the mean SI for that voxel in the four preexercise images. Cluster analysis was restricted to the superficial and deep compartments of the anterior tibialis muscle (AT/S and AT/D, respectively) and the extensor digitorum longus (EDL) muscle. As discussed above, when calculating M_{ij} , the difference in SI between the two voxels being compared was scaled to the range of muscle SIs encountered. To set the boundaries for this analysis, the user set a lower threshold that eliminated voxels containing only noise or in which there was incomplete fat suppression by the EPI sequence and an upper threshold that eliminated voxels containing blood vessels. Cluster analysis was performed with $T = 0.75$ and $K = 4$. For simplicity, the presentation and discussion of results is restricted to large clusters.

Traditional mfMRI analyses were also performed. SI was measured in ROIs drawn around the AT/S, AT/D, EDL, and soleus (Sol) muscles as a function of exercise or postexercise duration. The ROIs were defined by using of the high-resolution anatomic images; data from the functional images were obtained by converting the indexes into the image matrices from 256 × 256 image space to 64 × 64 image space. Registration errors were corrected by manually aligning the image mask of the mfMRI images with the anatomic images.

The relative SI changes and the contrast-to-noise ratio (CNR) were calculated. CNR was calculated according to

$$\text{CNR} = \frac{(S_1 - S_2)}{S_N} \quad (4)$$

where S_N is the noise standard deviation outside of the image mask and S_1 and S_2 are the SI values in the same ROI at two different times or in two adjacent ROIs at the same time.

Statistical Analysis

Statistical calculations were made with Microsoft Excel 97. To test for persistent effects of the prior exercise on muscle T2, the mean raw preexercise SI in the AT/S, AT/D, EDL, and Sol ROIs were compared by using a one-way ANOVA. To test for fatigue resulting from the prior exercise, the mean MVC values recorded before and after the perfusion imaging protocol were compared with a paired Student's *t*-test. To test for acute effects of the 2-min sustained dorsiflexion exercise on muscle T2, the relative change in SI was calculated between the first preexercise image and final exercise image and between the first preexercise image and the image in which the peak postexercise SI occurred. The mean relative SI changes were compared with a two-way ANOVA (muscle by time point), with repeated measures on time point, followed by Tukey's post hoc test. Mean and SE were calculated for all data. Statistical comparisons were considered significant at $P < 0.05$.

RESULTS

Simulation Studies

In all, 90 independent simulation trials were executed. Figure 3A shows the CA values for each condition; in 13 of 15 cases, the CA was 100% on each trial. In the other two conditions, the CA was ≥95%. Figure 3B shows the values of T required to produce these CA values. In general, setting T to 0.60 allowed correct discrimination between clusters. However, it was necessary to raise T for conditions A, D150, and E (see Fig. 3). In all cases, lower-than-optimum values of T produced clusters that were fewer in number and larger in size than programmed; the converse was true when T is set too high.

The algorithm was insensitive to values of $K > 2$, producing 100% CA for each of these trials. Values of $K \leq 2$ produced too many clusters, each smaller in size than the programmed regions (i.e., <25 voxels). Where possible, the merging procedure was implemented for these clusters. However, in most cases, the clusters were characterized as large (≥5 voxels) and therefore ineligible for the merging procedure.

Experimental Studies

Force production. The mean MVC before the perfusion-sensitive imaging protocol was 175.5 ± 25.4 N; this did not differ significantly from the mean MVC (174.3 ± 15.3 N) recorded after the submaximal exercise protocol ($P > 0.05$). All subjects were able to maintain the specified contraction intensity of 40% MVC for 2 min.

Traditional mfMRI analysis. Before the 2-min sustained dorsiflexion exercise, there were no statistically

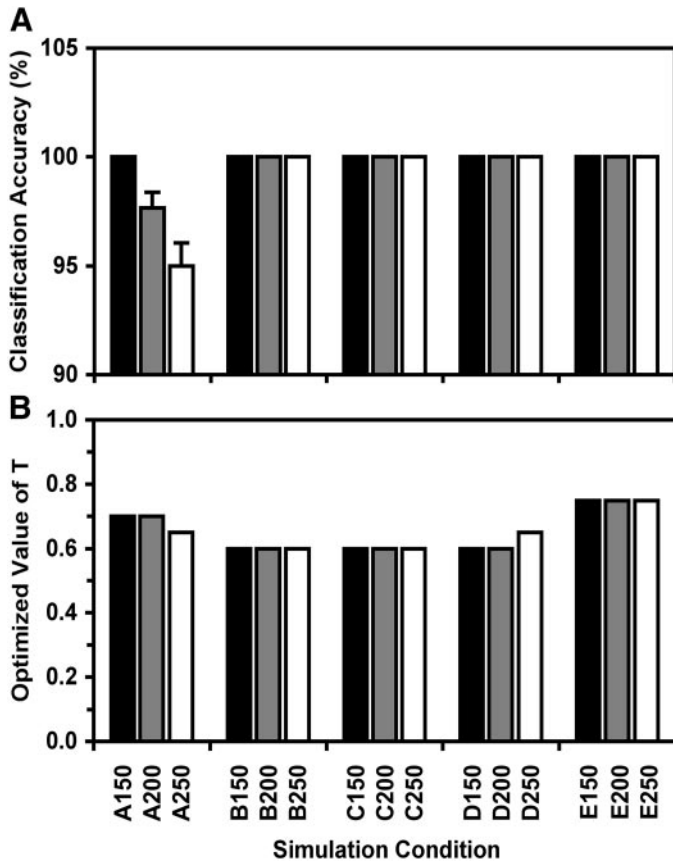


Fig. 3. Results of testing the algorithm with simulated data sets. A: classification accuracy (mean, SE). B: optimized values of the similarity threshold (T). Data are provided for the indicated simulation conditions, each at 3 different levels of signal-to-noise ratio (SNR). The data were obtained by using the simulated data sets described in the text, Fig. 2, and Table 1.

significant differences in mean raw SI among the AT/S, AT/D, EDL, and Sol ROIs ($P > 0.05$). In the final exercise image, there were increases in normalized SI of 5.6 ± 1.3 , 6.5 ± 0.9 , and $5.1 \pm 1.4\%$ in the ROIs drawn around the AT/S, AT/D, and EDL muscles ($P < 0.01$), which did not differ from each other. All differed from the Sol muscle ($P < 0.01$), in which the relative SI change ($-0.9 \pm 0.5\%$) was not significantly different from zero. After exercise, the peak relative increases in mean normalized SI in the AT/S, AT/D, and EDL ROIs were 14.1 ± 2.0 , 13.6 ± 1.9 , and $10.5 \pm 3.9\%$, respectively. These values did not differ from each other but were greater ($P < 0.01$) than the corresponding values for these ROIs at the end of exercise. The SI in the Sol remained unchanged ($P > 0.05$).

Clustering results: exercise. The clustering algorithm was implemented on the six subjects having acceptable data (i.e., free of visually apparent registration errors from image-to-image). Figure 4 shows an example exercise clustering result. Four clusters were identified in this subject: one in the EDL, one in the AT/D, and two in the AT/S. The filtered mean SI time courses of each cluster are shown in the insets and illustrate the two general patterns described earlier (Fig. 1). Each cluster in the AT had an abrupt initial rise of varying

magnitude followed by an early dip (like curves A–C in Fig. 1), whereas the cluster in the EDL had an early dip without an abrupt initial rise (like curve D in Fig. 1).

Exercise clustering results and the ROI data from the traditional mfMRI analysis are summarized for all subjects in Table 2. In 16 cases, there were relative SI changes in the user-defined ROIs that represented a CNR (relative to the preexercise images) > 5 . In 14 of these cases, one or more clusters were found. Eleven of the clusters were located in the AT and five were located in the EDL. The initial rise was absent in four of the five clusters in EDL and present in 12 of 13 clusters in the AT.

Clustering results: postexercise. The clustering algorithm was implemented in all subjects; an example clustering result from the postexercise data is shown in Fig. 5. In this subject, there was a single postexercise cluster that extended over the AT and EDL muscles.

Table 3 shows the postexercise cluster data for all of the subjects and reveals that, in five of six subjects, there was only one cluster. Table 3 also shows that in 15 of 16 cases in which the pre- to postexercise CNR was > 5 , a corresponding cluster was found. In all cases, the SI time courses were similar in shape to the inset to Fig. 5, although the time of the postexercise peak SI varied considerably from subject to subject (range of 28–116 s, mean of 79.3 ± 13.6 s).

DISCUSSION

mfMRI provides unique opportunities for characterizing muscle involvement during exercise. The robust (up to ~30%; Ref. 16) changes in SI that occur during and after exercise are intensity dependent (14) and relate directly to electromyographic measures of motor unit activation (1). The inherent spatial localization capability of MRI means that muscle utilization can be evaluated in both superficial and deep muscles with in-plane resolutions of $< 10 \text{ mm}^2$ by using EPI or $< 5 \text{ mm}^2$ by using conventional spin-echo imaging. However, the dynamic and complex changes in the volumes and the inherent T2 values of the three major tissue water compartments (intracellular, interstitial, and vascular), and possibly the rates of exchange between them, produce a complicated and incompletely understood SI time course.

To investigate how this time course is produced and to use the data in functional studies, it is necessary to organize the SI time courses from the many voxels in an ROI into a small number of groups. One approach is to make a series of a priori hypotheses about the functional organization of the active muscles; the user then draws ROIs according to the proposed organization scheme. An alternative is to build ROIs out of voxels whose SI time courses are similar to each other, reducing the number of prior hypotheses about anatomic or functional compartmentation.

Model-independent analytic approaches, such as principal component analysis (7) and fuzzy C-means

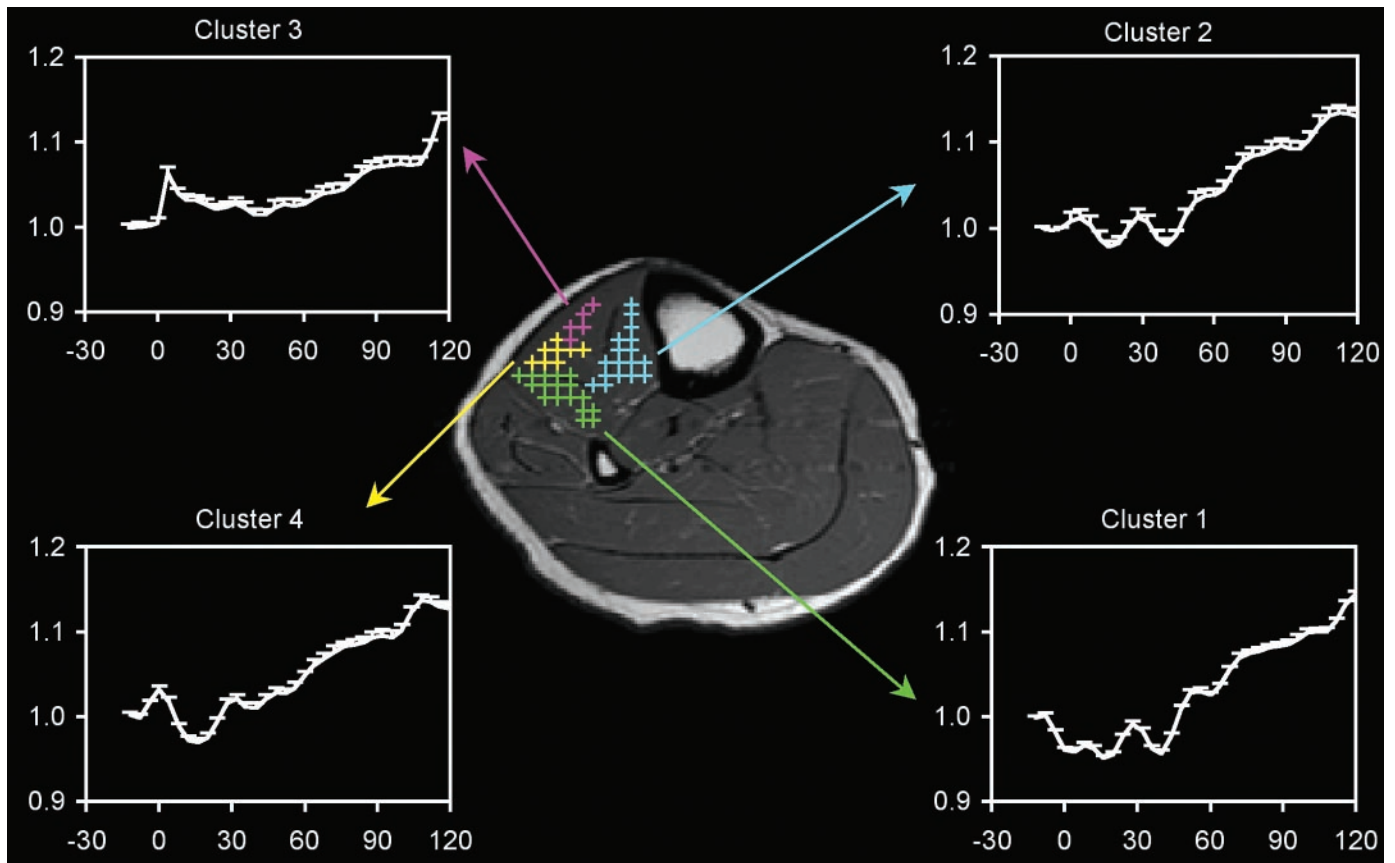


Fig. 4. Cluster analysis of mfMRI data acquired from *subject 5573* during exercise. Four clusters are seen: *cluster 1* is located in the extensor digitorum longus (EDL), *cluster 2* is located in the deep anterior tibialis muscle (AT/D), and *clusters 3 and 4* are located in the superficial anterior tibialis muscle (AT/S). In the insets, the mean SI time course for each cluster is shown as a function of exercise duration (in seconds); error bars indicate the SE.

clustering (3, 17), have been applied previously to brain functional MRI data. However, we know of only one prior implementation of model-independent activation detection that used mfMRI data (28). That study presented a method for detecting activated muscle based on histogram analysis and morphological processing; no fine partitioning of the activated muscles into different compartments was performed. The algorithm that we present in this work employs a hierarchical clustering technique to group mfMRI data into clusters on the basis of similarity in adja-

cent voxels. It is model independent and does not require the number of clusters to be known a priori, the latter being a typical requirement of fuzzy C-means clustering. The similarity calculation uses standard arithmetic and statistical calculations (ratio, mean, and Pearson product-moment correlation) and can be executed quickly (<5 min per subject, including interactive steps). We have used this method to demonstrate a functional separation in one or more of the contributors to the SI time course in mfMRI.

Table 2. Cluster and traditional analysis of mfMRI obtained during exercise

Subject	Cluster Analysis		Traditional Analysis		
	Number	Location	AT/S	AT/D	EDL
5572	3	AT/S (2) AT/D	8.7	17.9	0.0
5573	4	AT/S (2) AT/D EDL	23.2	20.9	20.8
5574	4	AT/S (2) AT/D EDL	20.6	9.3	26.2
5639	4	AT/S AT/D EDL (2)	7.8	7.0	8.0
6122	3	AT/S AT/D EDL	12.5	14.6	7.8
6394	0	N/A	0.6	11.7	6.7

For cluster analysis, the number and locations of the clusters are given; vertical lines separate unique clusters. For traditional analysis, the contrast-to-noise (CNR) between the end-exercise and preexercise images for the user-specified regions of interests (ROIs) is given. N/A, not applicable; AT/S, superficial anterior tibialis; AT/D, deep anterior tibialis; EDL, extensor digitorum longus; mfMRI, muscle functional MRI.

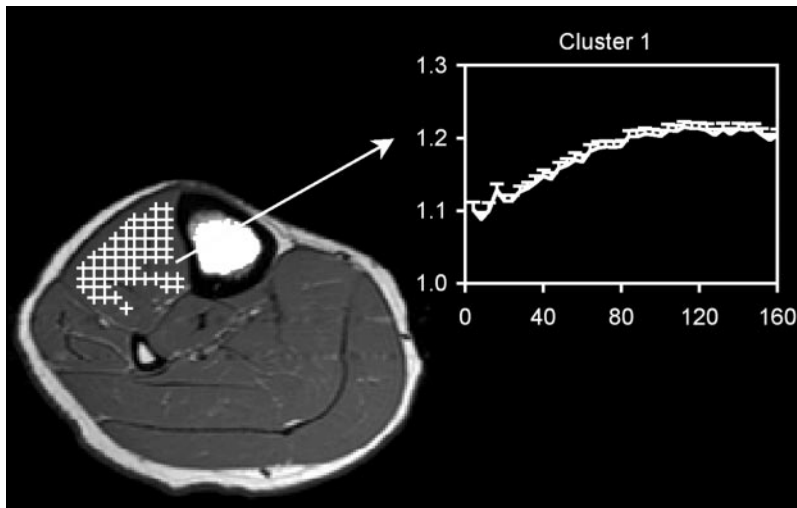


Fig. 5. Cluster analysis of mfMRI data acquired from *subject 5573* after exercise. One cluster, located in the AT/D, AT/S, and EDL, is seen. *Inset*: mean SI time course for the cluster as a function of postexercise duration in seconds; error bars indicate the SE.

There Were No Persistent Effects of the Prior Exercise

Before subjects performed the 2-min isometric dorsiflexion exercise that was used for testing the clustering algorithm, the subjects had performed a series of exercise and cuff occlusion protocols during which perfusion-sensitive images were acquired. Although the contractions were brief (10 s each) and there was a 5-min period of rest between each of them, it is still possible that these contractions fatigued the muscles or increased the T2 of the active muscles. In either case, it could influence the interpretation of the mfMRI data. However, there was no evidence that the prior exercise protocol affected the T2 of the AT and EDL or caused them to fatigue.

Traditional mfMRI Analysis Reveals General Patterns of Muscle Utilization

We observed that the changes in end-exercise SI of ~6% in the AT/S, AT/D, and EDL muscles did not differ significantly from each other. This finding is similar to that of Price et al. (20) who observed that, during isotonic dorsiflexion exercise performed with a resistance equal to 25% MVC, the SI change in the EDL does not differ significantly from that in the AT. The findings of our traditional mfMRI analysis differ from

those of Akima et al. (2) who found that, during isotonic dorsiflexion exercise performed with a resistance equivalent to 60% MVC, the SI change in the AT/S muscle is significantly greater than that of the AT/D muscle. After exercise, the SI increased to ~12% above the preexercise SI, which is similar to that observed in other studies (2, 5, 15, 19). The peak postexercise SI occurred ~80 s after exercise in the present study, slightly longer than in previous reports (~60 s to ~75 s; Refs. 2, 5, 15, 19). Overall, the results of our traditional mfMRI analysis agree generally with those of previous studies, although different exercise types (isotonic vs. isometric) and exercise intensities preclude a strict quantitative comparison.

The specific physiological meaning that should be ascribed to these changes is still open for debate. However, one conclusion to be drawn from our traditional mfMRI analysis is that there were no functional differences among the three regions of the anterior compartment measured. The clustering algorithm that we employed, however, indicates otherwise.

Clustering Algorithm Distinguishes Between Regions Whose SI Time Courses Differ

In experimental studies, we encountered two qualitatively different types of SI time courses and heterogeneity in the relative changes in SI at end exercise. To test the clustering algorithm realistically, these characteristics were replicated in the simulated data sets. In particular, the spatial distribution of the regions allowed each active region to border at least one voxel from the other three active regions and two the inactive regions. Therefore, within each data set, all possible combinations of magnitude and shape variation were tested. The CNRs between active and inactive regions ranged from 3.7 to 37.5, whereas the CNR between active regions ranged from zero (for adjacent regions having identical end-exercise SI changes but different SI time courses) to 31.3. In all cases, the algorithm performed with a mean CA of 95% or better.

Table 3. *Cluster and traditional analysis of mfMRI obtained after exercise*

Subject	Cluster Analysis		Traditional Analysis		
	Number	Location(s)	AT/S	AT/D	EDL
5572	1	AT	17.3	17.5	-2.8
5573	1	AT and EDL	55.2	47.6	55.2
5574	2	AT EDL	32.6	36.6	49.2
5639	1	AT and EDL	26.9	26.7	27.2
6122	1	AT	27.7	27.6	9.9
6394	1	AT	19.4	15.5	3.0

For cluster analysis, the number and locations of the clusters are given; vertical lines separate unique clusters. For traditional analysis, the CNR between the peak postexercise and preexercise images for the user-specified ROIs is given.

CA of 100% was attained on all trials with CNRs of 6.25 or higher.

To attain this level of accuracy, T and K must be set appropriately. When the CNR between the regions that one wishes to discriminate is greater than ~ 7.5 , setting T to 0.60 is indicated (Fig. 3B). However, when the anticipated CNR falls below this level, T must be raised (0.70 or higher; Fig. 3B) to avoid erroneous cluster connections due to noise. The algorithm is insensitive to values of K larger than 2 and has a low sensitivity to Gaussian noise. Filtering, merging small clusters into large clusters if their mean SI time courses are sufficiently similar, and/or raising T ameliorate the effects of low SNR. The algorithm is sensitive to misregistration errors caused by bulk tissue motion; however, this is true of traditional mfMRI analysis as well.

In the simulated data sets, the algorithm distinguished between inactive regions and active regions with great facility: in no case was a voxel from an inactive region of the simulated data set assigned to an active cluster. The reason for this is that the only SI variations in the inactive regions were those due to random noise, whereas those in the active regions underwent systematic variation according to the polynomial functions. The correlation coefficient in this case will be zero or close to zero. Thus, although the magnitudes of two SI time courses may be quite similar (as is the case when an inactive voxel borders a marginally active voxel), their low value for R_{ij}^2 will cause S_{ij} to fall below the clustering threshold. As a result, the inactive voxel will be excluded from the cluster.

The other purpose that incorporating the R^2 term into S serves is to act together with M in discriminating between regions that have similar end-exercise SI changes but very different behaviors in the early portion of the time course. Changing how S is calculated can alter the relative importance of this term. Using R^3 instead of R^2 will increase the dynamic range of S and increase its importance relative to the magnitude calculation; using R instead of R^2 has opposite effects on dynamic range and relative importance. In those cases, the optimized values of T reported in Fig. 3B will no longer hold. In both the simulated and experimental data sets, the ability to discriminate between different SI time course shapes was critical to the separation of functionally distinct clusters.

Clustering Algorithm Makes Fine Distinctions Between Neighboring Active Regions

There are two a priori hypotheses included in the implementation of the algorithm. The first is explicit and results from restricting the cluster analysis to a user-defined region. This requires that the user select those regions of the image in which activation is visually apparent. Expanding the ROI to intentionally include inactive regions would not significantly impact the results, because in several subjects there were regions with zero or near-zero changes in SI in both the exercise and postexercise data (Tables 2 and 3). In

none of these regions was a cluster found. This restriction is therefore not an essential element of the method; it could be removed, at the cost of increased computational time (~ 40 -fold for these data sets). Alternatively, clustering could be combined with the automatic activation detection method described by Warfield et al. (28) to eliminate the need for this restriction altogether.

The second assumption is implicit and involves how T is set. Because the understanding of the mfMRI time course is still incomplete, a "physiologically appropriate" value for T is unknown. However, we note that an important use of the algorithm will be in future mechanistic mfMRI studies, where it will be used to identify regionally varying SI time courses in muscle. This will allow spatial correlation of the SI time course with other regionally variant physiological parameters altered during exercise. For this purpose, setting T to 0.75 is appropriate because it made very subtle distinctions in SI time series (for examples, *clusters 1* and *2* in Fig. 4).

The clusters that resulted from the exercise data tended to follow anatomic boundaries: in most subjects, one or two clusters were found in the AT/S, one cluster was found in the AT/D, and one cluster was found in the EDL. In general, clusters were identified in regions having CNR > 5 in the traditional mfMRI analysis. The failure of clusters to appear in some cases of CNR > 5 may have resulted from bulk tissue motion or a value of T that was set too high for the noise level; however, the overall agreement was excellent.

However, the two methods disagreed with respect to the existence of functional differences between the regions: the cluster analysis suggests that such differences exist (in most subjects, there were three or four unique clusters identified in the anterior compartment), whereas the traditional analysis suggested the opposite (the relative end-exercise SI changes were not significantly different among the regions). The major source of this discrepancy is the sensitivity (cluster analysis) or lack of sensitivity (traditional analysis) to the initial rise and other elements of the early SI time course (< 60 s). The sensitivity of the clustering algorithm to the entire time series, as well as the ability to identify regionally varying time series in a model-independent manner, indicates that cluster analysis may be a more useful approach to identifying the mechanism of the mfMRI response than traditional analysis.

Regional Functional Differences Are Not Seen in the Postexercise Data

With regard to the postexercise data, when comparing the existence of clusters in regions that had CNR > 5 in the traditional mfMRI analysis, the agreement between the two methods was also excellent. In this case, the methods agreed further with regard to the apparent absence of functional differences between the regions: traditional analysis found no significant differences between the mean SI changes in the AT/S,

AT/D, and EDL. Similarly, in five of six subjects, cluster analysis of postexercise data identified only a single cluster. (In aside, the existence of a single cluster in postexercise data that encompassed the AT/S, AT/D, and EDL indicates that the cluster distinctions observed during exercise did not arise from partial volume artifacts caused by muscle boundaries.)

There are two possible explanations for the difference between the cluster analysis of exercise and postexercise data. One is that there are new physiological determinants of SI in mfMRI that emerge after exercise or determinants that are active during exercise are absent afterward. The other possibility is that the identities of physiological determinants of SI are the same during and after exercise but that the relative contributions differ during these two time periods. In either case, the implications of the data are twofold: first, they suggest that, after moderate-intensity isometric contractions, SI in mfMRI may be dominated by a single contributor that is regulated globally across previously active muscles, such as postexercise hyperemia (12). Second, they indicate that analyzing exercise vs. postexercise data could yield different conclusions about functional distinctions between and within individual muscles.

What Does the Cluster Differentiation Mean?

Above, we noted that, in both simulated and experimental data sets, an important source of cluster discrimination came from the early part of the SI time course. In particular, the magnitudes (and even the existence) of the initial rise and the early dip were quite variable between clusters. To evaluate what functional significance this may hold, we first discuss the possible meanings of these portions of the early mfMRI SI time course.

With regard to the initial rise, it is noteworthy that we used a single-slice acquisition with a TR that was insufficient for full recovery of longitudinal magnetization. Under these conditions, the spins inside the imaged volume will be partially saturated and those outside of it will be essentially unsaturated, and muscle shortening would contribute to the initial rise. Muscle shortening occurs even in isometric muscle contractions (13), and the resulting introduction of unsaturated spins into the slice plane would immediately increase the signal by up to ~4% (for a T_1 of 1.2 s and muscle shortening equal to or greater than the slice thickness).

Dips in SI of ~1% have also been reported in the early portion of the brain functional MRI time course and have been attributed to local oxygen consumption that exceeds oxygen supply (29, 30). The oxygen supply-demand mismatch causes early elevations in microvascular deoxyhemoglobin concentration, which have been observed with optical spectroscopy (10); these changes decrease the blood T2 (27). In muscle, optical spectroscopy has shown that, during sustained isometric dorsiflexion exercise at 30% MVC, there is a rapid increase in oxygen extraction, with blood oxygen-

ation reaching a plateau at an exercise duration of ~45 s (11). A local minimum in the mfMRI time course occurs at an exercise duration of 20–30 s (Fig. 4; Refs. 2, 19). The lack of full temporal correspondence between blood oxygenation changes and the early dip in SI in mfMRI may result from the simultaneous, large-magnitude increase in the T2 of the tissue parenchyma.

If muscle shortening and oxygen extraction do contribute to the initial rise and subsequent dip, respectively, then these portions of the mfMRI SI time course should be considered when attempting to discriminate between functionally distinct regions of muscle. One specific implication of the cluster data is that, if the hypothesis concerning the role of shortening in the initial rise is correct, then the characteristic appearance of the initial rise in the AT but not the EDL muscle would indicate that the AT muscle was shortening (and, presumably, producing force) significantly, whereas the EDL was not. This proposal is consistent with the AT muscles' role as the prime mover in dorsiflexion (26). The meaning of the cluster differentiation with regard to later elements of the SI time course is unclear because they are likely generated by multiple, unmeasured physiological quantities (such as perfusion, oxygen extraction, and metabolic characteristics) whose relative contributions are unknown.

Overall, the fact that cluster analysis distinguished between the AT/S and the AT/D means that our data tend to agree with the conclusions of Akima et al. (2) concerning recruitment plasticity in the AT. However, the only conclusion that we can make with confidence is that the SI time courses of each cluster differ. Other conclusions based on the proposed contributions of muscle shortening, blood oxygenation changes, and energy metabolism to the SI time course are speculative. As noted above, presently, the main value of the algorithm is that it will be a useful tool for testing these hypotheses.

Summary and Conclusions

In this study, we have presented a method for detecting functionally distinct clusters of mfMRI data that require no a priori model of neuromuscular organization. The method was tested in simulated data sets and applied to experimental data obtained during and after isometric dorsiflexion exercise. The clustering algorithm made distinctions between anatomically, and possibly functionally, distinct regions of the leg's anterior compartment that were not seen in traditional mfMRI analysis. The increase in sensitivity in the cluster analysis results from its use of more data (the full SI time course) in its functional classifications. Both types of analysis showed that, under these experimental conditions, the major determinants of mfMRI SI after exercise are similar in the AT and EDL muscles. These analyses further suggest that mfMRI data obtained after exercise, rather than during exercise, may lack information that could be used to identify contributions to the mfMRI response.

We thank Peter Brown for technical assistance and Terri Hickey, Ian Lanza, Cheryl McMurray, Dr. David Russ, Hedy Sarofin, and Ted Towse for their assistance with data collection.

DISCLOSURES

We acknowledge the following grant support: National Institute of Arthritis and Musculoskeletal and Skin Diseases Grant F32 AR-08614 (to B. M. Damon) and National Institute on Aging Grant R01 AG-21094 (to J. A. Kent-Braun).

REFERENCES

- Adams GR, Duvoisin MR, and Dudley GA. Magnetic resonance imaging and electromyography as indexes of muscle function. *J Appl Physiol* 73: 1578–1583, 1992.
- Akima H, Ito M, Yoshikawa H, and Fukunaga T. Recruitment plasticity of neuromuscular compartments in exercised tibialis anterior using echo-planar magnetic resonance imaging in humans. *Neurosci Lett* 296: 53–56, 2000.
- Baumgartner R, Scarth G, Teichtmeister C, Somorjai R, and Moser E. Fuzzy clustering of gradient-echo functional MRI in the human visual cortex. Part I: reproducibility. *J Magn Reson Imaging* 7: 1094–1101, 1997.
- Damon BM, Gregory CD, Hall KL, Stark HJ, Gulani V, and Dawson MJ. Intracellular acidification and volume increases explain R_2 decreases in exercising muscle. *Magn Reson Med* 47: 14–23, 2002.
- Disler DG, Cohen MS, Krebs DE, Roy SH, and Rosenthal DI. Dynamic evaluation of exercising leg muscle in healthy subjects with echo planar MR imaging: work rate and total work determine rate of T_2 change. *J Magn Reson Imaging* 5: 588–593, 1995.
- Fleckenstein JL, Haller RG, Lewis SF, Archer BT, Barker BR, Payne J, Parkey RW, and Peshock RM. Absence of MRI enhancement of skeletal muscle in McArdle's disease. *J Appl Physiol* 71: 961–969, 1991.
- Friston KJ, Frith CD, Liddle PF, and Frackowiak RS. Functional connectivity: the principal-component analysis of large (PET) data sets. *J Cereb Blood Flow Metab* 5: 5–14, 1993.
- Fung BM and Puon PS. Nuclear magnetic resonance transverse relaxation in muscle water. *Biophys J* 33: 27–37, 1981.
- Green RA and Wilson DJ. A pilot study using magnetic resonance imaging to determine the pattern of muscle group recruitment by rowers with different levels of experience. *Skeletal Radiol* 29: 196–203, 2000.
- Grinvald A, Frostig RD, Siegel RM, and Bartfeld E. High-resolution optical imaging of functional brain architecture in the awake monkey. *Proc Natl Acad Sci USA* 88: 11559–11563, 1991.
- Hicks A, McGill S, and Hughson RL. Tissue oxygenation by near-infrared spectroscopy and muscle blood flow during isometric contractions of the forearm. *Can J Appl Physiol* 24: 216–230, 1999.
- Hu L, Fleckenstein JL, and Babcock E. Perfusion MRI of post-exercise muscle (Abstract). *Proceedings of the International Society for Magnetic Resonance in Medicine 10th Scientific Meeting*, Honolulu, Hawaii, 2002, p. 290.
- Ito M, Kawakami Y, Ichinose Y, Fukushima S, and Fukunaga T. Nonisometric behavior of fascicles during isometric contractions of a human muscle. *J Appl Physiol* 85: 1230–1235, 1998.
- Jenner G, Foley JM, Cooper TG, Potchen EJ, and Meyer RA. Changes in magnetic resonance images of muscle depend on exercise intensity and duration, not work. *J Appl Physiol* 76: 2119–2124, 1994.
- Kennan RP, Price TB, and Gore JC. Dynamic echo planar imaging of exercised muscle. *Magn Reson Imaging* 5: 935–941, 1995.
- Kerviler ED, Leroy-Willig A, Jehenson P, Duboc D, Eyraud B, and Syrota A. Exercise-induced muscle modifications: study of healthy subjects and patients with metabolic myopathies with MR imaging and P-31 spectroscopy. *Radiology* 181: 259–264, 1991.
- Moser E, Diemling M, and Baumgartner R. Fuzzy clustering of gradient-echo functional MRI in the human visual cortex. Part II: quantification. *J Magn Reson Imaging* 7: 1102–1108, 1997.
- Ploutz-Snyder LL, Nyren S, Cooper TG, Potchen EJ, Meyer RA. Different effects of exercise and edema on T_2 relaxation in skeletal muscle. *Magn Reson Med* 37: 676–82, 1997.
- Price TB, Kennan RP, and Gore JC. Isometric and dynamic exercise studied with echo planar magnetic resonance imaging (MRI). *Med Sci Sports Exerc* 30: 574–580, 1998.
- Price TB, McCauley TR, Duleba A, Wilkens KL, and Gore JC. Changes in magnetic resonance transverse relaxation times of two muscles following standardized exercise. *Med Sci Sports Exerc* 27: 1421–1429, 1995.
- Prior BM, Ploutz-Snyder LL, Cooper TG, and Meyer TA. Fiber type and metabolic dependence of T_2 increases in stimulated rat muscles. *J Appl Physiol* 90: 615–623, 2001.
- Saab G, Thompson RT, and Marsh GD. Effects of exercise on muscle transverse relaxation determined by MR imaging and in vivo relaxometry. *J Appl Physiol* 88: 226–233, 2000.
- Saab G, Thompson RT, and Marsh GD, Picot PA, and Moran GR. Two-dimensional time correlation relaxometry of skeletal muscle in vivo at 3 Tesla. *Magn Reson Med* 46: 1093–1098, 2001.
- Sjogaard G, Adams RP, and Saltin B. Water and ion shifts in skeletal muscle of humans with intense dynamic knee extension. *Am J Physiol Regul Integr Comp Physiol* 248: R190–R196, 1985.
- Sloniger MA, Cureton KJ, Prior BM, Evans EM. Lower extremity muscle activation during horizontal and uphill running. *J Appl Physiol* 83: 2073–2079, 1997.
- Snell RS. *Clinical Anatomy for Medical Students*. Boston, MA: Little, Brown, 1995, p. 556–557.
- Spees WM, Yablonskiy DA, Oswood MC, and Ackerman JJ. Water proton MR properties of human blood at 1.5 Tesla: magnetic susceptibility, T_1 , T_2 , T_2^* , and non-Lorentzian signal behavior. *Magn Reson Med* 45: 533–542, 2001.
- Warfield SK, Mulkern RV, Winalski CS, Jolesz FA, and Kikinis R. An image processing strategy for the quantification and visualization of exercise-induced muscle MRI signal enhancement. *J Magn Reson Imaging* 11: 525–531, 2000.
- Yacoub E and Hu X. Detection of the early negative response in fMRI at 1.5 Tesla. *Magn Reson Med* 41: 1088–1092, 1999.
- Yacoub E, Shmuel A, Pfeuffer J, Van De Moortele PF, Adriany G, Ugurbil K, and Hu X. Investigation of the initial dip in fMRI at 7 Tesla. *NMR Biomed* 14: 408–412, 2001.
- Yoshioka H, Anno I, Kuramoto L, Matsumoto K, Jikuya T, and Itai Y. Acute effects of exercise on muscle MRI in peripheral arterial occlusive disease. *Magn Reson Imaging* 5: 651–659, 1995.